Supplementary Figures

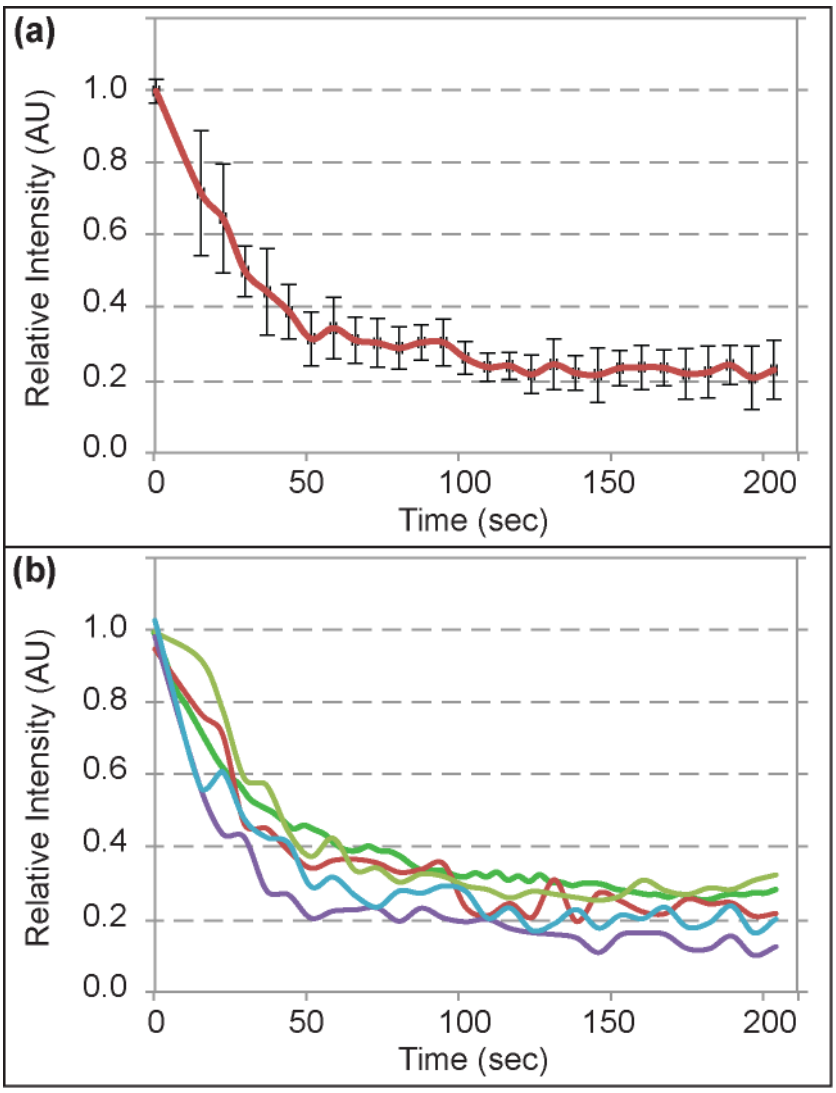

Supplementary Figure S1. Inhibition kinetics of p53/HDM2 binding induced by Nutlin 3 on live cells. Reproducibility of the p53/HDM2 binding disruption kinetics induced by Nutlin 3 measured using the F3H binding assay at the *LacO* array. BHK cells containing a stably integrated *LacO* array were transiently transfected with pNeG-p53(NTD), pCAG-mCh-HDM2(NTD) and GBP–LacI. In (a) is shown the mean and standard error of the time lapse quantification of the relative binding of HDM2 to p53 after drug treatment. The assay was performed in quintuplicates. In (b) are shown the individual time lapse traces of each single experiment of the five repeats.

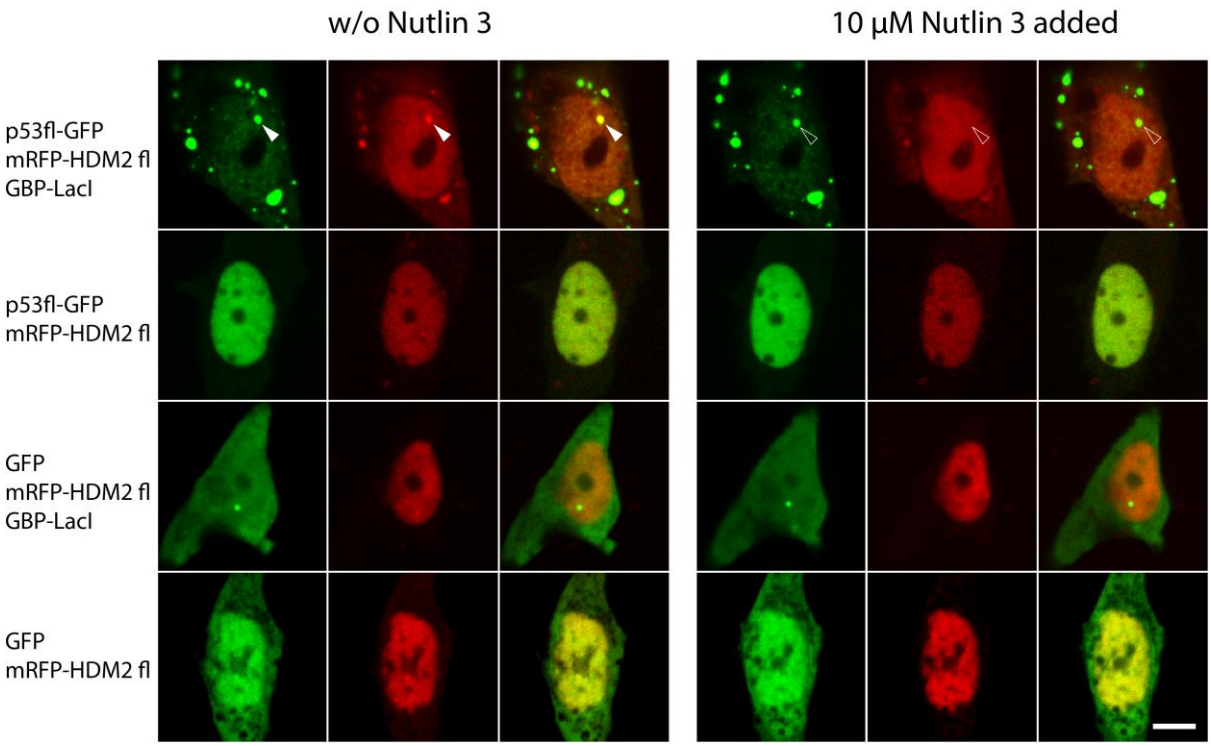

Supplementary Figure S2. Full length p53, HDM2, GFP and mCherry proteins do not show unspecific binding to the *LacO* array. Images of live BHK cells co-transfected with full-length p53-GFP, full-length Ch-HDM2 and GBP-LacI are shown (the first row). Ch-HDM2 colocalized with p53-GFP at the *LacO* spot (filled arrowhead). After treatment with 10 µM Nutlin 3, the Ch-HDM2 was released from the *LacO* spot (open arrowhead). GFP control and control without GBP-LacI were performed to exclude unspecific binding. Scale bar, 5 µm.

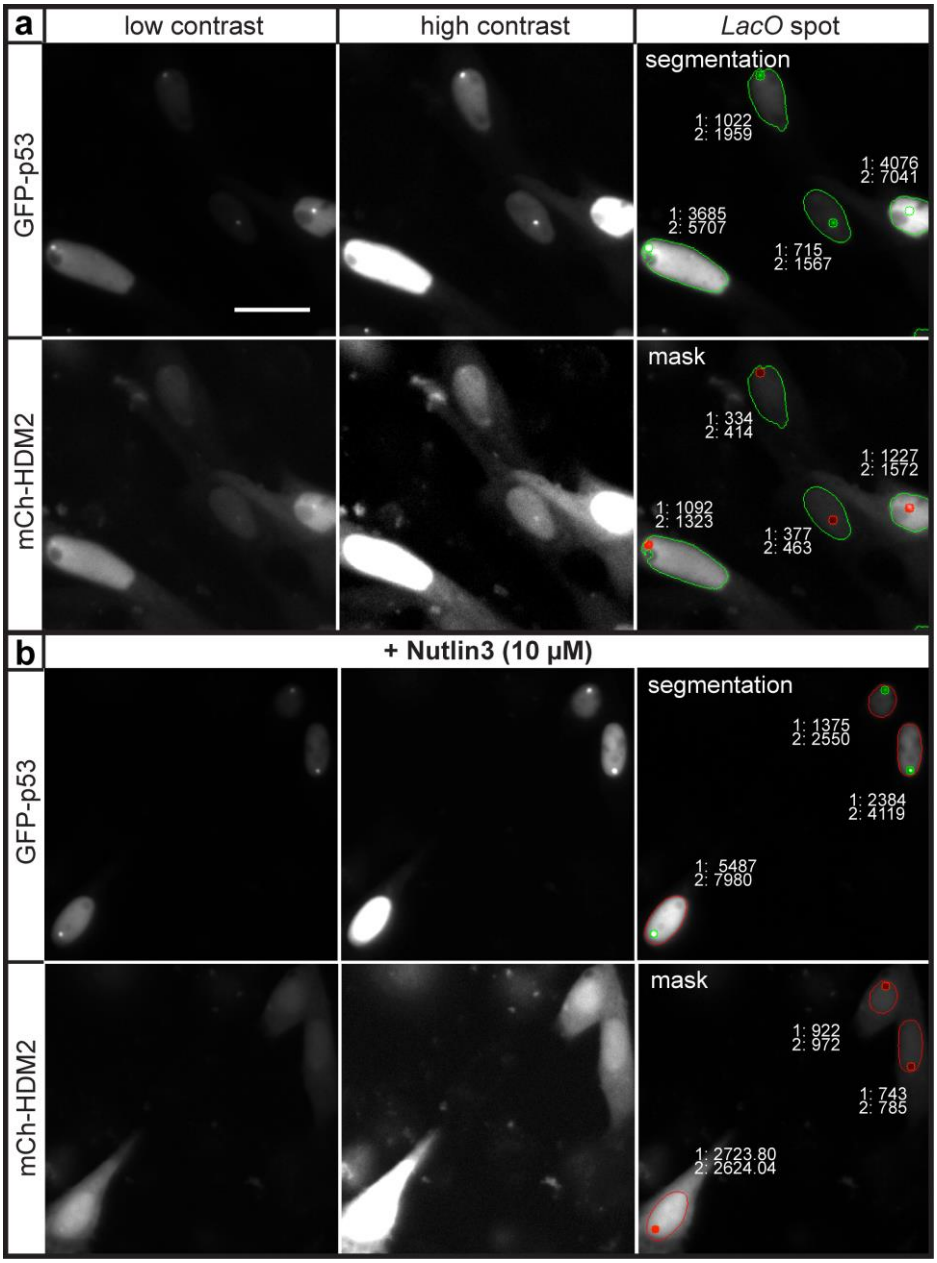

Supplementary Figure S3. Automated wide field image detection and analysis of protein-protein interactions at the *LacO* array can be made over a wide range of protein expression levels. Shown are BHK cells co-expressing GBP-LacI, GFP-p53 (pNeG-p53 (NTD), upper panel, a, b) and mCh-HDM2 (pCAG-mCh-HDM2 (NTD), lower panel, a, b). Low and high contrast images (left and middle, respectively) are presented to highlight heterogeneous protein levels. On the right is shown the automated intensity threshold segmentation of nucleus and *LacO* spot regions. Green (a) and red (b) nucleus borders indicate classification as interaction-positive and interaction-negative cells, respectively. Mean fluorescence intensities of nucleus (1) and spot (2) regions (16 bit grayscale) are indicated. Scale bar, 10 µm.

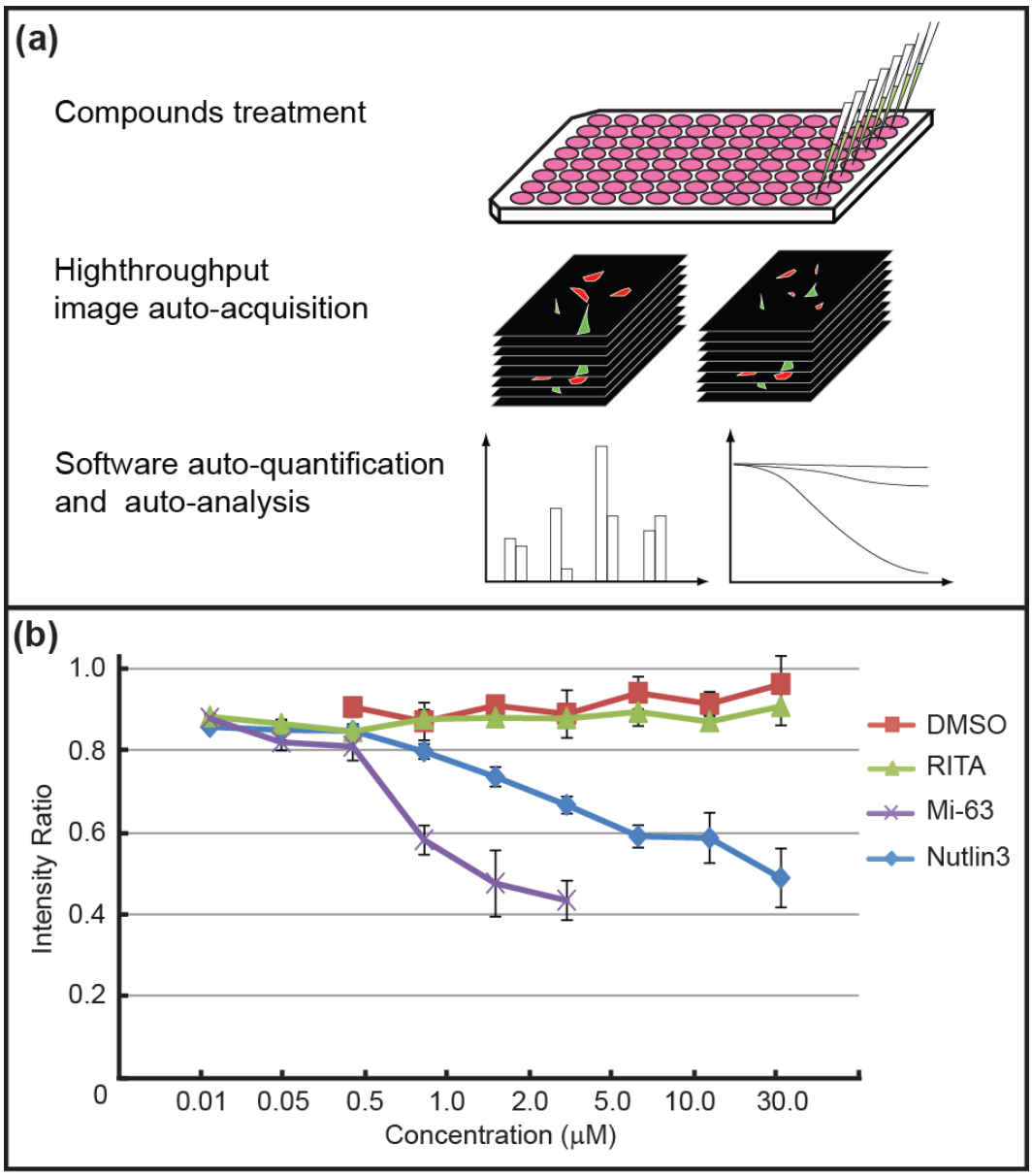

Supplementary Figure S4. Comparative analysis of drug efficacy on disrupting protein interactions. High throughput screening. (a) Cells were seeded onto a 96-well plate and treated with Nutlin 3, Mi-63 and RITA at the concentrations indicated. Cells were fixed and images acquired automatically using a Perkin Elmer Operetta imaging platform. The intensity ratio of mCh/GFP at the *LacO* spot in each cell was measured. (b) mCh/GFP intensity ratio of p53 and HDM2 at the *LacO* spot when treated with different concentrations of DMSO (control), RITA, Mi-63 and Nutlin 3. Mi-63 has a stronger inhibiting effect than Nutlin 3, while RITA does not hinder the interaction between p53 and HDM2. Technical triplicates were performed, and the normalized mean percentage with standard error of the mean are shown. The total number of positively triple transfected cells analyzed per data point was 1,200. The present test required 37,200 positively triple transfected cells obtained out of a total of 316,000 imaged cells.

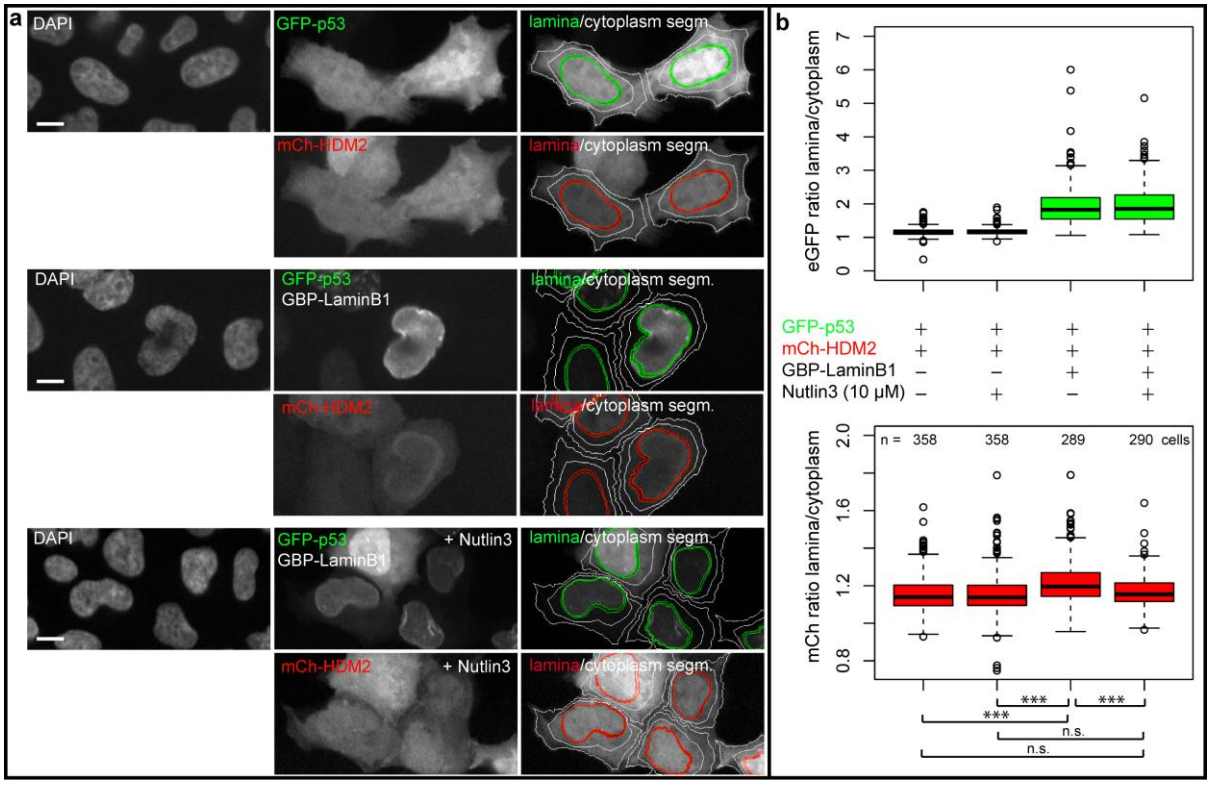

Supplementary Figure S5. Automated wide field image acquisition and analysis of protein-protein interactions at the nuclear lamina using the GBP-LaminB1. Images were acquired using the confocal mode of an automated Perkin Elmer Operetta imaging platform. The assay was performed in HeLa cells using an NLS-free version of GFP-p53 (pCAG-eGFP-p53) and mCh-HDM2 (pCAG-mCh-HDM2). (a) The proteins display a diffuse distribution throughout the cells upon co-expression (upper panel). Triple-transfection with GBP-LaminB1 causes GFP-p53 recruitment at the nuclear lamina and co-recruitment of mCh-HDM2 (middle panel). Nutlin3 treatment causes diffuse redistribution of mCh-HDM2 (lower panel). For quantitative analysis, a laminar ROI (red or green) and a cytoplasmic ROI (white) were automatically segmented (right side). Scale bars, 10 µm. (b) Box plot representations of eGFP (top) and mCherry (bottom) intensity ratios between the lamina and the cytoplasm ROIs in absence and presence of GBP-LaminB1 and in absence and presence of Nutlin3. Medians are shown as solid black lines and the top and bottom box ends represent upper and lower quartiles, respectively. Whiskers represent the minimal and maximal data points within the 1.5x interquartile range. Data sets were tested for significance with an unpaired t-test ($p<0.001$). The number of cells analyzed is indicated above the boxplot diagram.

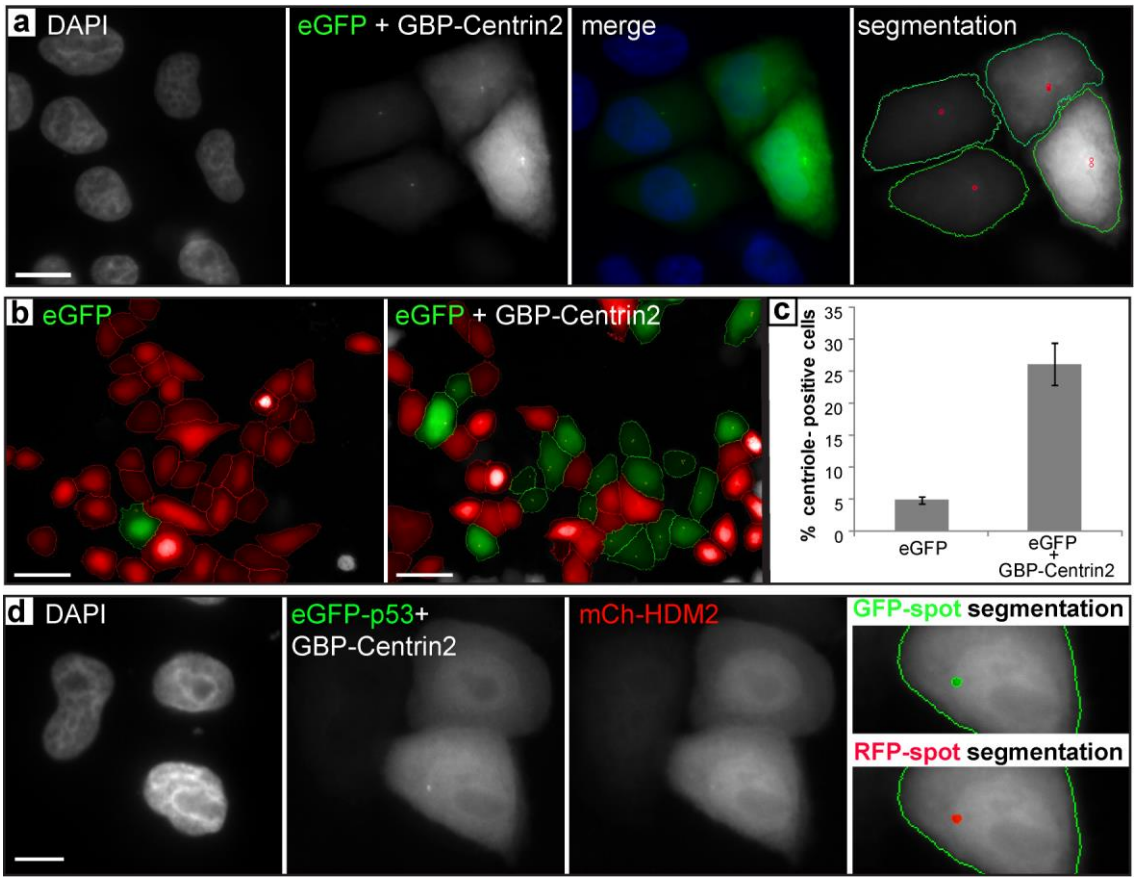

Supplementary Figure S6. Automated wide field image detection and analysis of protein-protein interactions at the centriole (cytoplasm) using the GBP-Centrin2 construct. (a) HeLa cells co-expressing GBP-Centrin2 and eGFP at different expression levels allowing automated intensity threshold segmentation of centriolar eGFP localization in the cytoplasm. Images were acquired using an automated Perkin Elmer Operetta imaging platform. Scale bar, 10 µm. (b, c) Quantitative, automated image analysis. Green segmentation masks indicate classification of centriole-positive cells, red indicates classification of centriole-negative cells. Scale bar, 50 µm. The error bars represent the standard deviation from technical triplicates. The shown data are a representative depiction from three independent transfection experiments. (d) Centriolar recruitment of eGFP-p53 (pCAG-eGFP-p53) and mCh-HDM2 (pCAG-mCh-HDM2) and intensity threshold based spot segmentation in both the eGFP and mCherry channel. Scale bar, 10 µm.

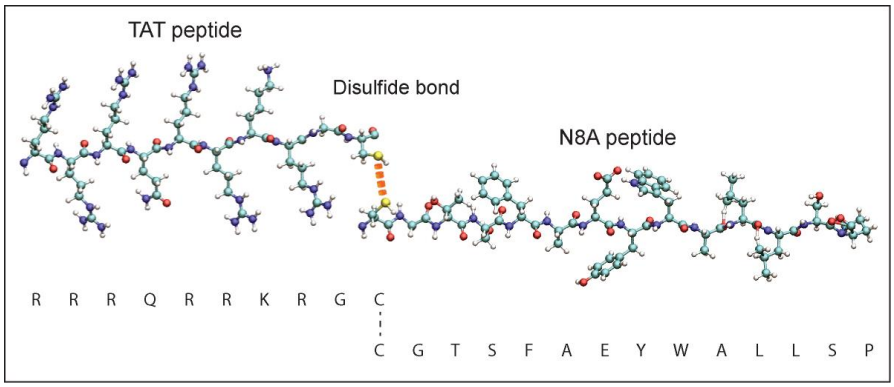

Supplementary Figure S7. Sequence and stretched structure of the TAT peptide coupled by a disulfide bridge to the N8A peptide inhibitor.

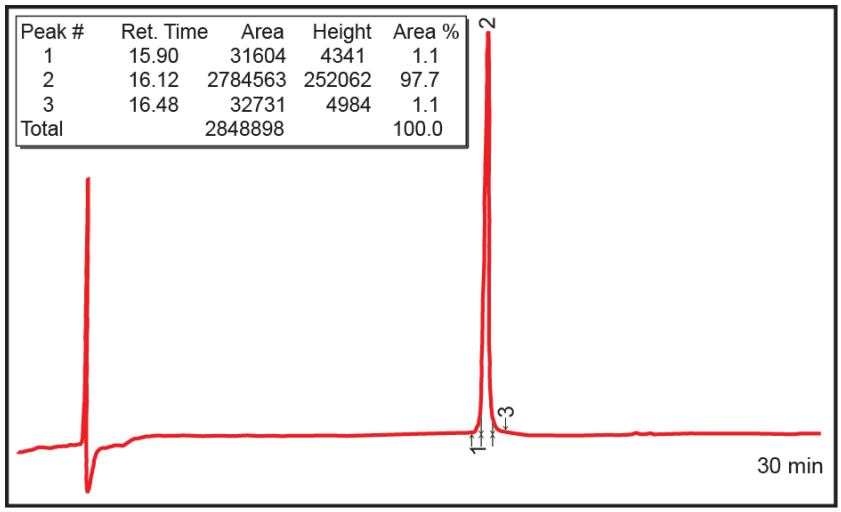

Supplementary Figure S8. Analytical HPLC chromatogram of the N8A peptide coupled through a disulfide bridge to the TAT peptide.

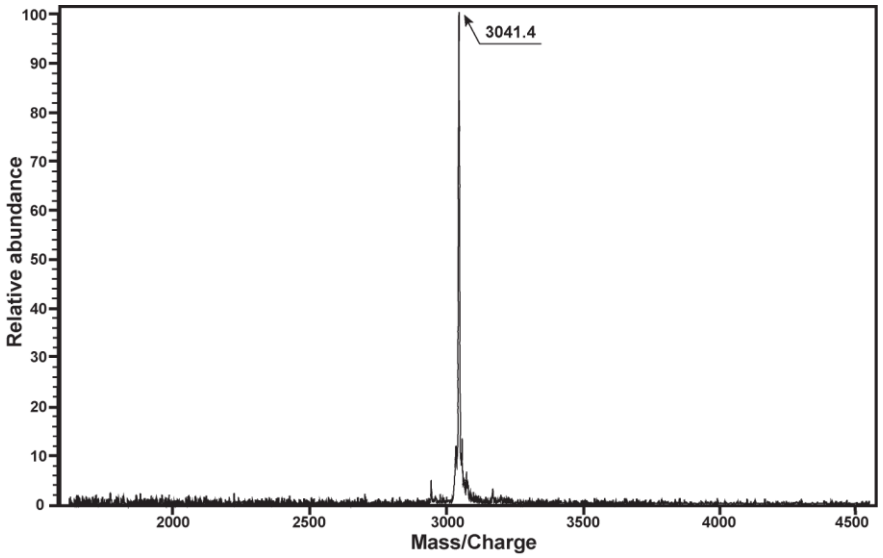

Supplementary Figure S9. Mass spectrum of the N8A peptide coupled through a disulfide bridge to the TAT peptide.

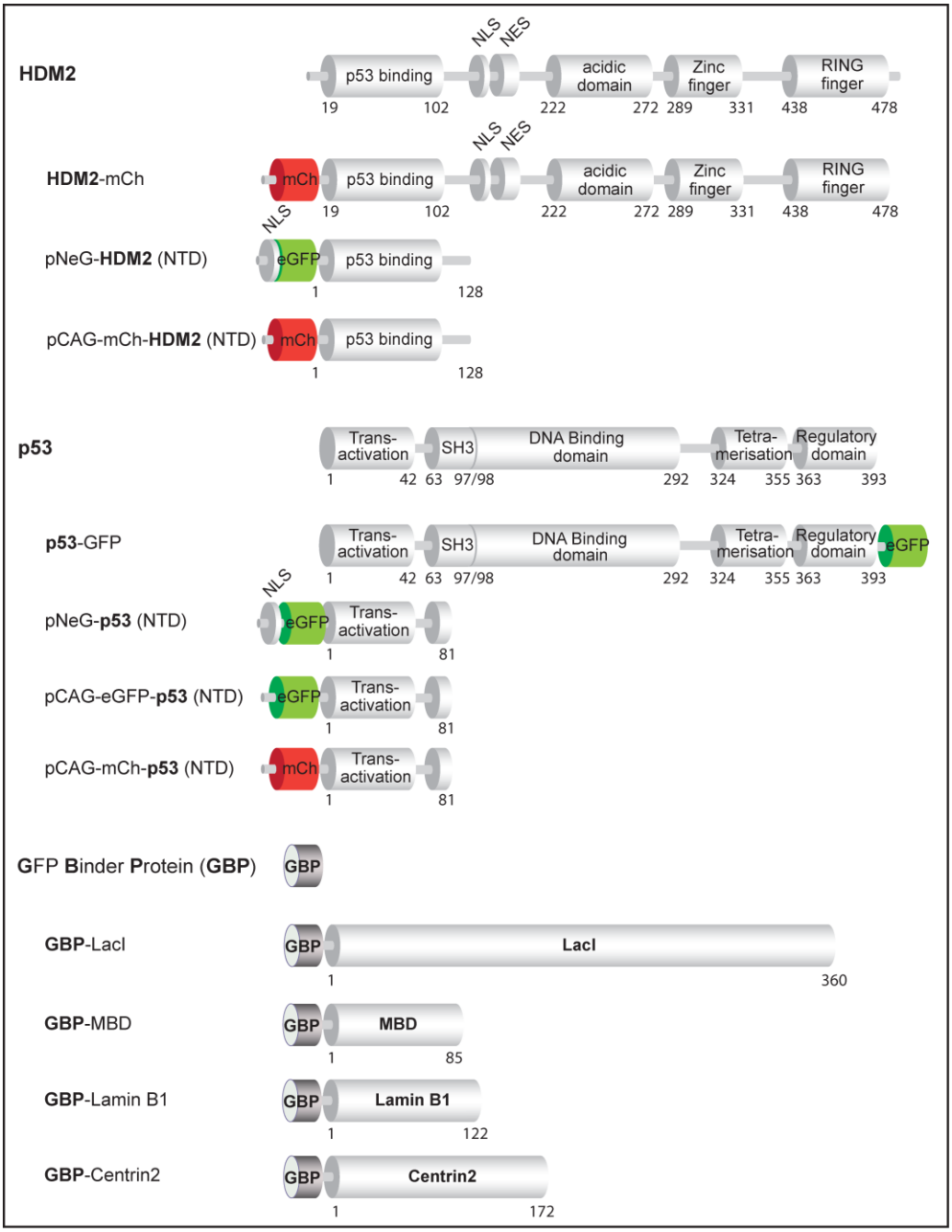

Supplementary Figure S10. Summary of chimeric fusion proteins. Schematic representation of the human HDM2, human p53 and llama derived **G**FP **B**inder **P**rotein (GBP) together with the corresponding chimeric fusion protein constructs.

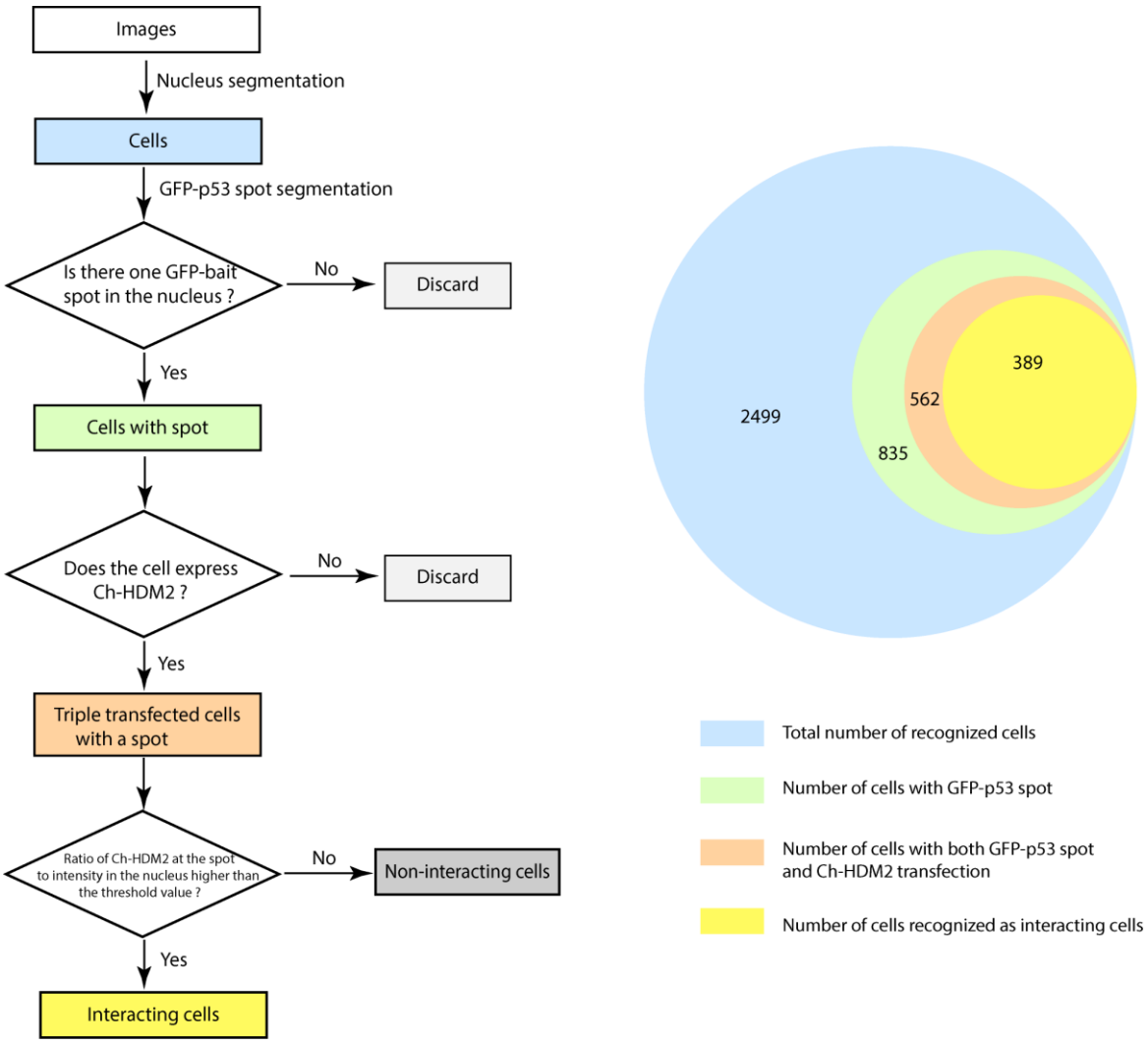

Supplementary Figure S11. Analysis flow diagram and cell populations of the high throughput assay using the GBP-LacI system. On the left, flow diagram of the high throughput analysis protocol. Cells are heuristically analyzed and divided into different groups. Cells in all the groups are evaluated, and the information, such as numbers and fluorescence intensities are measured. On the right, classification and number of cells in each group analyzed in one well. In this well, 30 fields were imaged and analyzed. From these 30 images, a total of 2,499 cells are recognized, about 33% (835 cells) of which are with one GFP-p53 spot in the nucleus. In the cells with a GFP-p53 spot, approximate 67% (562 cells) express mCh-HDM2. In these 562 cells, 389 about 70% are automatically recognized as interacting cells. In this context it should be mentioned that the prior establishment of stable cell lines changes these statistics as practically all cells become informative.